

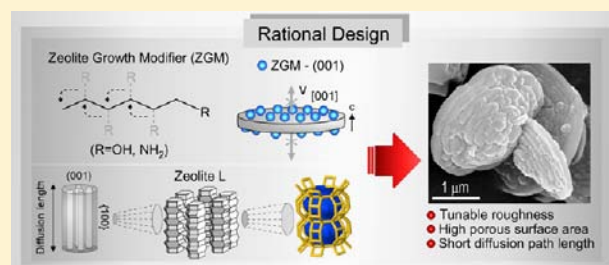
A Facile Strategy To Design Zeolite L Crystals with Tunable Morphology and Surface Architecture

Alexandra I. Lupulescu, Manjesh Kumar, and Jeffrey D. Rimer*

Department of Chemical and Biomolecular Engineering, University of Houston, Houston, Texas 77204-4004, United States

S Supporting Information

ABSTRACT: Tailoring the anisotropic growth rates of materials to achieve desired structural outcomes is a pervasive challenge in synthetic crystallization. Here we discuss a method to selectively control the growth of zeolite crystals, which are used extensively in a wide range of industrial applications. This facile method cooperatively tunes crystal properties, such as morphology and surface architecture, through the use of inexpensive, commercially available chemicals with specificity for binding to crystallographic surfaces and mediating anisotropic growth. We examined over 30 molecules as potential zeolite growth modifiers (ZGMs) of zeolite L (LTL type) crystallization. ZGM efficacy was quantified through a combination of macroscopic (bulk) and microscopic (surface) investigations that identified modifiers capable of dramatically altering the cylindrical morphology of LTL crystals. We demonstrate an ability to tailor properties critical to zeolite performance, such as external porous surface area, crystal shape, and pore length, which can enhance sorbate accessibility to LTL pores, tune the supramolecular organization of guest–host composites, and minimize the diffusion path length, respectively. We report that a synergistic combination of ZGMs and the judicious adjustment of synthesis parameters produce LTL crystals with unique surface features, and a range of length-to-diameter aspect ratios spanning 3 orders of magnitude. A systematic examination of different ZGM structures and molecular compositions (i.e., hydrophobicity and binding moieties) reveal interesting physicochemical properties governing their efficacy and specificity. Results of this study suggest this versatile strategy may prove applicable for a host of framework types to produce unrivaled materials that have eluded more conventional techniques.



INTRODUCTION

The development of facile techniques capable of rationally designing crystalline materials with tailored properties is a ubiquitous challenge that spans an array of applications in the chemical, pharmaceutical, and electronics industries. The ability to *a priori* tune crystallization in order to produce desirable structural features is a nontrivial task that requires a discerning proficiency for controlling the anisotropic kinetics of crystal growth. In many instances, the need to concurrently regulate multiple properties (without altering the intrinsic crystal structure) calls for innovative optimization strategies. A notable example is the synthesis of zeolite crystals^{1–5} where subtle changes in synthesis conditions can induce polymorphism⁶ and alter crystal size and habit in ways that are often unpredictable. As such, there is a preeminent need to develop synthetic routes capable of overcoming these challenges toward a realization of material design objectives.^{2,4}

The well-ordered pores of LTL crystals serve as conduits for shape-selective catalysis and nanochannel hosts for ion, metal, or molecule inclusion, mass transport, and/or occlusion. Furthermore, their optical transparency can be beneficial in detection and sensor devices. Over the past 20 years zeolite L (LTL type) has attracted attention for applications in catalytic processes,^{7–12} ion-exchange and separations,^{13,14} and photonic devices, such as FRET-sensitized solar cells,¹⁵ luminescent solar

concentrators (LSCs),¹⁶ and color changing media.¹⁷ Moreover, functionalized zeolite L organic–inorganic hybrids have been explored for use in biomedical applications, including diagnostic¹⁸ and imaging devices,¹⁹ drug delivery vectors,²⁰ and cell array scaffolds.^{21,22}

Conventional LTL synthesis yields cylindrical crystals with one-dimensional channels (ca. 0.7 nm aperture) oriented along the *c*-axis (or [001]) length of the cylinder (see Figure 1a,d). The performance of LTL crystals in the aforementioned applications relies heavily upon their physical characteristics, such as crystal size, morphology (i.e., length-to-diameter aspect ratio), and surface roughness, as well as their chemical properties, such as acidity and ion-exchange capacity. Calzaferri has shown that low aspect ratio (disc-like) LTL crystals in photonic devices produce higher trapping efficiency.¹⁷ Disk-like shapes can also facilitate *c*-oriented layering for the preparation of thin-film technologies, while high aspect ratio (rod-like) crystals can be useful as microcapillary devices for light harvesting antenna and luminescent labeling.²³ In some applications, it is desirable to tailor more than one property. Exemplary cases in catalysis include aromatization reactions involving Pt-LTL catalysts where some groups^{9,10} report that

Received: February 11, 2013

Published: April 9, 2013

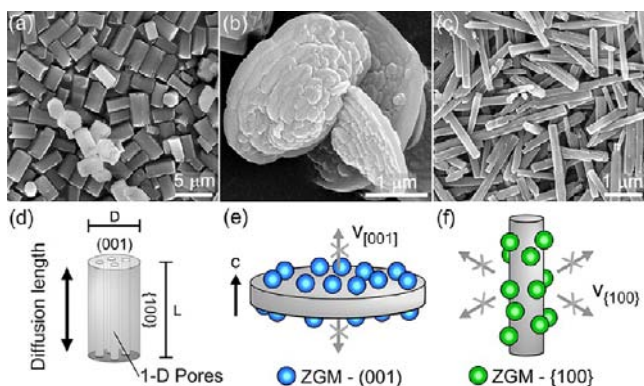


Figure 1. Electron micrographs of zeolite L crystals prepared with the following synthesis conditions: (a) control (absence of ZGMs), (b) butylamine, A4 (10 wt%), and (c) poly(diallyldimethylammonium chloride), PDDAC (2.1 wt%). The schematic in (d) illustrates that the path length for sorbate diffusion in zeolite LTL channels is proportional to the [001] length L , while sorbate access to pore openings is dependent on the (001) surface area, or diameter D . (e) ZGMs that preferentially bind to the (001) surface reduce the diffusion path length along the c -axis. (f) ZGM binding to {100} surfaces increases the LTL crystal aspect ratio, L/D .

increased external surface area of LTL crystals exudes a greater influence on catalytic performance, while others^{8,10} argue that reduced pore length has a more significant impact on activity. These observations allude to a more widespread realism that disparate applications often require distinct zeolite properties. Establishing structure–function relationships to delineate optimal zeolite properties necessitates the development of synthesis techniques capable of achieving set design objectives. This motivates the need for new platforms adept at precisely tailoring crystal size, morphology, and surface features.

Past studies report the effects of adjusting synthesis parameters,^{8,24–28} such as water, temperature, and alkali content, to produce zeolite L crystals of varying morphology ranging from 30 nm particles²⁹ to micrometer-sized cylinders (with length-to-diameter aspect ratios spanning 0.2–13).^{26,30} Other studies have examined the incorporation of organic additives in zeolite growth solutions, such as surfactants,³¹ ligands (e.g., triethanolamine and bis-tris),³⁰ and cosolvents (e.g., ethanol, diols, etc.).^{32,33} Organic additives have been used in the synthesis of a variety of zeolite framework types, including (but not limited to) LTL,^{32–34} mordenite (MOR),³⁵ offretite (OFF),³⁶ zeolite A (LTA),³⁷ and silicalite-1 (MFI).^{31,38,39} Several mechanisms describing the role of organic additives have been postulated on the basis of thermodynamic and kinetic arguments. Some groups have suggested that organics influence the anisotropic rates of growth by altering the surface free energy of zeolite crystals, while others hypothesize that organic complexation (or sequestration) of soluble silicate or aluminosilicate species alters the nature of available growth units.^{35,40} A common function of organics in zeolite synthesis is their role as structure-directing agents (SDAs). Organic SDAs and so-called space fillers (i.e., a subcategory of SDAs) are typically selected with a size and shape commensurate with zeolite pores, cages, or channels.⁴¹ Only a small fraction of zeolites (including LTL) crystallize in the absence of organic SDAs, whereas the vast majority of framework types require organics to facilitate the formation of building units (e.g., oligomers, rings, cages, etc.). The use of novel SDAs^{2,42,43} and space fillers⁴⁴ has proven to

be an effective method to modify zeolite crystal size and habit, and to produce new structures.

In a previous study we examined the crystallization of MFI-type zeolite in the presence of organics, termed zeolite growth modifiers (ZGMs). We attributed the effect of ZGMs to a well-known mechanism whereby organic molecules alter the anisotropic rates of crystallization.⁴⁵ The general mechanism^{46,47} invoked for ZGMs involves physisorption of modifiers to specific crystal surfaces, which inhibits the attachment of incoming building units, thereby reducing the growth rate normal to the surface. This phenomenon occurs in a wide range of natural and synthetic crystallization processes. For instance, modifiers are pervasive in biological systems, such as shell and bone formation, where ions, proteins, and other biomolecules often serve as moderators of crystal nucleation and growth.^{48–52} Additional examples include biomimetic modifiers of calcification,^{49,50} antifreeze proteins,^{53,54} drugs for various diseases,^{55,56} mineralization inhibitors in the oil and gas industry,⁵⁷ and the design of synthetic metal oxides (e.g., TiO₂).⁵⁸

Here we explore the use of ZGMs in zeolite L synthesis as a versatile strategy to improve the control of crystal habit and surface architecture (i.e., topography and external surface area). We demonstrate an ability to produce LTL crystals with remarkably small diffusion path length (<100 nm) and concomitant large (001) surface area (1–10 μm²/particle). We use a combination of characterization techniques, including electron microscopy, X-ray diffraction, and atomic force microscopy, to examine the influence of commercial ZGMs on LTL crystal morphology and surface properties. Furthermore, we explore the physicochemical factors of ZGM efficacy and specificity through systematic investigation of their molecular structure and composition. In this study, we analyze more than 30 polyols and amines in order to develop a more comprehensive understanding of structure–function relationships governing ZGM effectiveness. Herein we discuss the results of these studies and identify heuristic guidelines for tuning ZGM-zeolite L molecular recognition.

EXPERIMENTAL SECTION

Materials. The following chemicals from Sigma-Aldrich (St. Louis, MO) were used as reagents for zeolite syntheses: LUDOX (40 wt% suspension in water), potassium hydroxide (85% pellets), and aluminum sulfate hydrate (98%). The following chemicals from Sigma-Aldrich were used as growth modifiers in zeolite syntheses: ethanol (200 proof), 1-propanol (ACS reagent, ≥ 99.5%), 1-butanol (ACS reagent, ≥ 99.4%), 1-pentanol (≥99%), 1-hexanol (≥98%), 1,2-butanediol (98%), 1,2-pentanediol (96%), 1,5-pentanediol (purum, ≥ 97% (GC) Fluka), 1,2-hexanediol (98%), 1,2,3-hexanetriol (BIO-XTRA, ≥98.0%), 1,2,6-hexanetriol (96%), ethylene glycol (99%), 1,2-propanediol (99.5%), glycerol (≥99.5%), diethyl ether (anhydrous, ≥99.7%), dimethoxymethane (reagent plus, 99%), 1,2-dimethoxyethane (≥99.5% (GC)), poly(diallyldimethylammonium chloride) (MW 150K, 20%), 1-ethyl-1-methylpyrrolidinium bromide (99%), propylamine (≥99%), butylamine (99.5%), hexamethylenediamine (98%), triethyleneglycol (≥99%), (R/S)-1,3-butanediol (99%), tributylphosphine oxide (95%), and triethylenetetramine (≥97%). The deionized water used in all experiments was purified with an Aqua Solutions RODI-C-12A purification system (18.2 MΩ). All reagents were used as received without further purification.

Zeolite Crystallization. LTL crystals were synthesized in the absence of a structure-directing agent using solutions with a molar ratio of 1.0 Al₂O₃:20 SiO₂:10.2 K₂O:1030 H₂O. Potassium hydroxide (0.69 g, 0.0104 mol) was first dissolved in water (ca. 7.6 g), followed by addition of aluminum sulfate hydrate (0.18 g, 0.00051 mol). This

solution was stirred until clear (ca. 5 min). LUDOX (1.53 g, 0.0102 mol) was then added dropwise, and the resulting solution was left to stir overnight at room temperature. Crystals synthesized by this procedure in the absence of growth modifier are referred to as the *control*. For studies of different zeolite growth modifiers, the modifier of choice was added in a molar ratio of 1.5 ZGM:1.0 SiO₂ (unless otherwise stated) to 10 g of growth solution (described above) yielding mixtures with a pH of 14.4 ± 0.2. The solution was placed in a Teflon-lined stainless steel acid digestion bomb and heated without mixing at autogenous pressure in an oven (ThermoFisher Precision Premium 3050 series gravity oven) for 3 days at 180 °C. The reaction product was isolated as a white powder (ca. 300 mg) by vacuum filtration using a 0.4-μm membrane (47 mm Whatman nuclepore polycarbonate track-etched membrane) with repeated deionized water washings. For the preparation of microscopy samples, a small amount of powder was redispersed in deionized water and shaken vigorously. An aliquot of this solution was then placed on a glass slide and dried overnight. All samples for microscopy studies were prepared via transfer of crystals from the glass slide to SEM or AFM sample holders. Elemental analysis of control crystals was performed by Galbraith Laboratories, Inc. (Knoxville, TN).

Zeolite Characterization. LTL samples were characterized by powder X-ray diffraction (XRD), thermogravimetric analysis (TGA), atomic force microscopy (AFM), and scanning electron microscopy (SEM). XRD patterns were collected on a Siemens D5000 X-ray diffractometer using Cu Kα radiation (40 kV, 30 mA). TGA experiments were conducted on a SDT Q600 thermogravimetric analyzer (TA Instruments). AFM analysis was performed on a MFP-3D-SA instrument (Asylum Research, Santa Barbara, CA). Tapping-mode images were obtained with 256 scans/line at an average scan velocity of 1.2 μm/s using Olympus AC240TS probes (2 N/m spring constant). SEM microscopy was conducted at the Methodist Hospital Research Institute in the Department of Nanomedicine SEM Core using a Nova NanoSEM 230 instrument with ultra-high-resolution FESEM (operated at 15 kV and a 5 mm working distance). All zeolite samples were coated with a 15 nm layer of Pt metal prior to imaging.

RESULTS AND DISCUSSION

A critical challenge in the application of our design approach is the identification of modifiers with molecular recognition for a specific crystal face. A strategic target for zeolite LTL design is the identification of ZGMs that selectively bind to the basal (001) surface, thereby producing thin platelets with reduced diffusion path length along the *c*-axis parallel to the 1D pores (see Figure 1e). In order to identify potential structural features capable of promoting zeolite-ZGM binding, we first examined the molecular topology of LTL crystal surfaces. Idealized (001) surfaces are drawn in Figure 2 according to the cleavage plane identified by Terasaki et al.^{59,60} in transmission electron micrographs of LTL crystals. Inspection of the basal plane reveals that the density of hydroxyl groups (either SiOH or AlOH) protruding from the top of double-6-membered ring (*d6R*) building units is much higher on the (001) surface (4.2 OH groups/nm²) compared to the {100} surfaces (1.5 OH groups/nm²). This implies that molecules with H-binding moieties are suitable ZGMs; however, the close proximity of hydroxyl groups also suggests steric hindrance may influence ZGM binding to each *d6R* unit. Furthermore, entropic contributions from hydrophobic segments of organic modifiers must be considered since ZGMs may adsorb on crystal surfaces with their alkyl backbone oriented parallel to the (001) plane and/or within pore openings, which can reduce the ordering of hydration layers surrounding CH₂ groups. Therefore, the molecules investigated in this study contain varying hydrophobic and isomeric H-binding constituencies. A select number

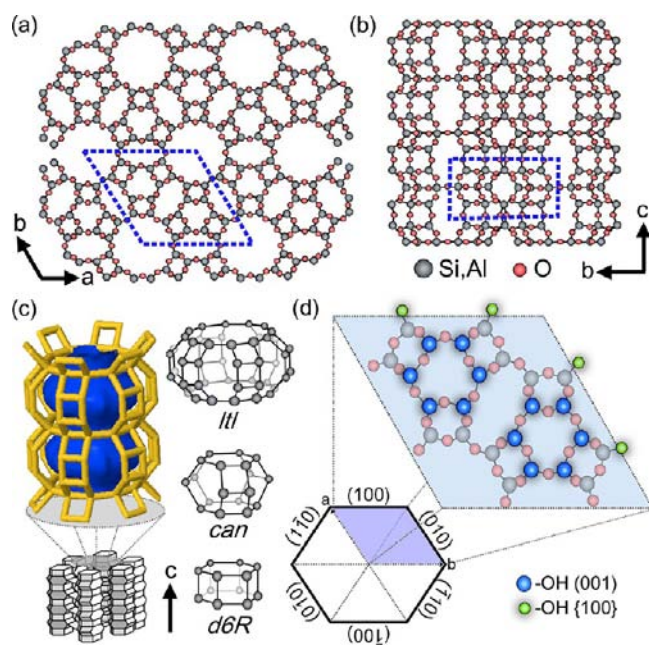


Figure 2. Hexagonal crystal structure of LTL-type zeolite (*P6/mmm* space group, $a = b = 1.81$ nm and $c = 0.76$ nm) viewed normal to the (a) basal (001) surface and (b) (100) surface. Dashed lines indicate a single unit cell. (c) LTL is comprised of 1D channels (12-membered ring aperture, ca. 0.7 nm) oriented axially along the *c*-axis. The channels are *ltl* cages derived from the connection of *can* and *d6R* building units. (d) The bulk crystal habit is a faceted cylinder with sides comprised of six symmetrically equivalent {100} surfaces. The projected unit cell identifies the positions of surface hydroxyl groups (SiOH or AlOH) on the pinacoidal (001) surface (blue circles) and six equivalent prismatic {100} surfaces (green circles).

of these modifiers are listed in Table 1, while a comprehensive list is provided in Table S1 in the Supporting Information (SI).

A nomenclature, LN_{*ijk*}, was formulated in order to facilitate discussion of ZGMs, where L = P for primary alcohols, D for diols, T for triols, and A for amines. *N* refers to the total number of carbons, and subscripts *ijk* refer to the location of alcohol or primary amine groups along the alkyl backbone. LTL crystals were prepared according to the procedure reported by Gomez et al.³³ using organic-free growth solutions. ZGMs were added prior to hydrothermal treatment in 50% molar excess (i.e., molar ratio ZGM/SiO₂ = 1.5). Herein we will refer to LTL crystals grown in the absence of modifiers as control samples. These syntheses consistently produced cylindrical crystals with a length-to-diameter aspect ratio of 1.7 ± 0.1 (Figure 1a). Interestingly, the majority of modifiers tested in this study preferentially adsorbed on the (001) surface, resulting in substantial changes to the LTL crystal morphology without inducing polymorphism (a common phenomenon in zeolite synthesis that can arise from the addition of organics). Powder XRD patterns of crystals extracted from growth solutions in the absence and presence of ZGMs reveal little, if any, crystal impurities. In Figure 3, the comparison of XRD patterns for modified LTL crystals prepared in solutions of P4, T6_{1,2,6}, and PDDAC and a reference pattern⁶¹ reveals that the ZGMs do not promote the formation of crystal polymorphs. Additional XRD patterns are provided in Figure S1 in the SI.

Distinct trends emerged when we plotted the aspect ratio of LTL crystals grown in the presence of ZGMs as a function of the logarithm of their octanol–water partition coefficient, or

Table 1. List of Alcohol and Amine Zeolite Growth Modifiers

Symbol	Name	Formula	MW (g·mol ⁻¹)	Structure
Alcohols: primary (P), diols (D), and triols (T)				
P2	ethanol	C ₂ H ₆ O	46.07	
D2 _{1,2}	ethylene glycol	C ₂ H ₆ O ₂	62.07	
P3	n-propanol	C ₃ H ₈ O	60.10	
D3 _{1,2}	1,2-propanediol	C ₃ H ₈ O ₂	76.09	
T3 _{1,2,3}	glycerol	C ₃ H ₈ O ₃	92.09	
P4	n-butanol	C ₄ H ₁₀ O	74.12	
D4 _{1,2}	1,2-butanediol	C ₄ H ₁₀ O ₂	90.12	
D4 _{1,3}	(R/S)1,3-butanediol	C ₄ H ₁₀ O ₂	90.12	
D5 _{1,2}	1,2-pentanediol	C ₅ H ₁₂ O ₂	104.15	
D5 _{1,5}	1,5-pentanediol	C ₅ H ₁₂ O ₂	104.15	
D6 _{1,2}	1,2-hexanediol	C ₆ H ₁₄ O ₂	118.17	
T6 _{1,2,3}	1,2,3-hexanetriol	C ₆ H ₁₄ O ₃	134.17	
T6 _{1,2,6}	1,2,6-hexanetriol	C ₆ H ₁₄ O ₃	134.17	
Amines: primary (A)				
A3	propylamine	C ₃ H ₉ N	59.11	
A4	butylamine	C ₄ H ₁₁ N	73.14	

log P , which is a standard convention used to quantify molecular hydrophobicity (see details of log P calculations in SI). Notably, the LTL crystal aspect ratio decreases linearly with increasing hydrophobicity (Figure 4, solid line). This trend holds true for modifiers with three or fewer carbons, which include polyols (D2_{1,2}, D3_{1,2}, and T3_{1,2,3}), alcohols (P2 and P3), and *n*-propylamine (A3). For instance, the aspect ratio monotonically decreases from glycerol, T3_{1,2,3} (2.09 ± 0.06), to *n*-propanol, P3 (0.5 ± 0.1). This observation is qualitatively consistent with past studies that describe the thermodynamics of polyol adsorption on zeolites at ambient conditions.^{62–66} These studies have shown that the adsorption constant, K_{ads} , increases as a function of polyol hydrophobicity,^{65,66} which may explain why ZGMs with higher log P values are more effective inhibitors of the LTL [001] growth rate. Moreover, it is evident from thermodynamic studies that polyols adsorb within zeolitic channels. While it has been proposed that the inclusion of organic space fillers within *lll* cages can influence the anisotropic rates of LTL growth,⁴⁴ the mode of action for ZGMs involves only organics bound to exterior crystal surfaces. Our estimates suggest the fraction of polyols within zeolite

pores is marginal, and that a majority of polyol molecules in the aqueous growth solution are available to bind to the exterior surfaces of LTL crystals. For example, if we assume the approximate uptake of *n*-butanol (P4) is 0.1 g/g zeolite (an upper estimate for LTL based on the value reported by Vlachos and Sandler⁶³ for P4 uptake in MFI-type zeolite), less than 5% of P4 (mass basis) resides within the 1D pores of LTL crystals. The remaining ca. 95% of ZGM would therefore be available in bulk solution, although a percentage of this ZGM may be sequestered by soluble silicates or aluminosilicates via the formation of organic–inorganic complexes. Interestingly, thermogravimetric analysis of extracted LTL powders reveals that a cursory washing with deionized water during zeolite filtration is sufficient to recover approximately 99% of ZGMs used in the synthesis solution (see Figure S2). This observation highlights the potential to recover and recycle ZGMs *a posteriori*, which has economic implications for the commercial viability of this approach.

Upon further examination of all ZGMs in Figure 4, an apparent threshold in modifier efficacy is observed when the length of their alkyl segments, $(\text{CH}_2)_n$, is around $n = 3$. Above

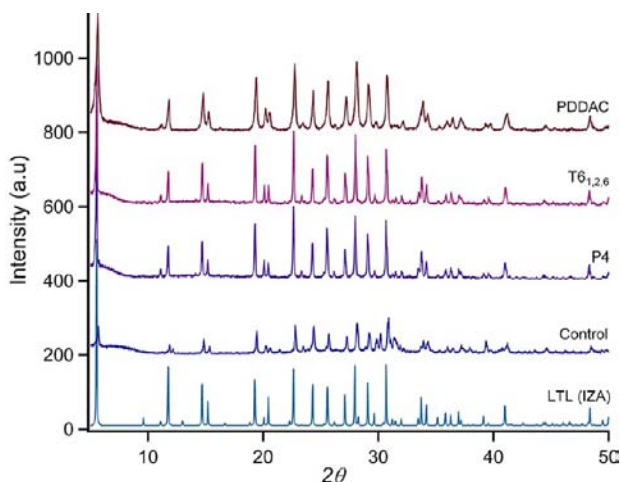


Figure 3. Powder XRD patterns of LTL crystals prepared in the absence of modifier (control) and with the following ZGMs: poly(diallyldimethylammonium chloride) (PDDAC), 1,2,6-hexanetriol ($T6_{1,2,6}$), and *n*-butanol (P4). Comparison of the experimental powder patterns with a simulated pattern for zeolite LTL (Linde type L, $[Na_3K_6(H_2O)_{21}][Si_{27}Al_9O_{72}]$) obtained from ref 61 (labeled as IZA) reveal trace, if any, crystal impurities.

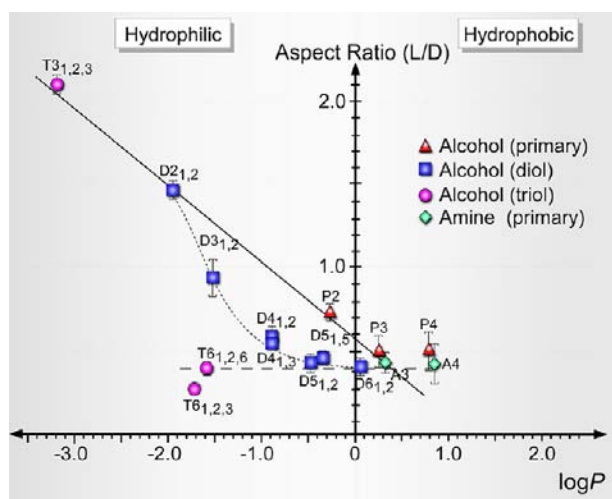


Figure 4. Effect of ZGM hydrophobicity (x -axis) on the length-to-diameter aspect ratio (y -axis) of LTL crystals. Primary alcohols, primary amines, diols, and triols with three or fewer carbons exhibit a linear dependence (solid line, $R^2 = 0.93$) with changes in the logarithm of the partition coefficient, $\log P$. The trend for diols of increasing alkyl length is nonlinear (dotted line), while the grouping of polyols with more than three carbons exhibits approximately no change in aspect ratio with increasing ZGM hydrophobicity (dashed line). Each data point is an average of three separate experiments with error bars equaling two standard deviations.

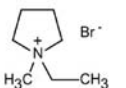
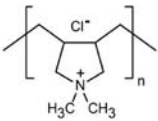
this value, ZGM efficacy is unaffected by the addition of carbons, or increased hydrophobicity. This threshold alkyl length is evident in several cases, including the disproportionate reduction in aspect ratio between $D3_{1,2}$ and $D4_{1,2}$ (i.e., molecules with $n < 3$) compared to the reduction between $D5_{1,2}$ and $D6_{1,2}$ (i.e., molecules with $n \geq 3$). For $1,k$ -diols, the progression from $D2_{1,2}$ to $D6_{1,2}$ results in a nonlinear decrease in aspect ratio (Figure 4, dotted line) with increasing carbon length (or $\log P$). Indeed, if we consider all ZGMs having consecutive $(CH_2)_n$ segments with $n \geq 3$ (Figure 3, dashed line), there is little variance in aspect ratio as a function of ZGM

hydrophobicity. As such, these studies reveal that hydrophobic (entropic) interactions between ZGMs and zeolite surfaces contribute to their efficacy for impacting LTL crystal habit; however, this correlation is less prominent when modifiers contain alkyl segments of $(CH_2)_3$ or longer.

In order to investigate additional contributions to ZGM efficacy, we examined the influence of both number and spatial arrangement of alcohol binding moieties on the alkyl backbones of polyols with segments of $(CH_2)_3$ or longer. Among the molecules tested, 1,2,3-hexanetriol ($T6_{1,2,3}$) produced LTL crystals with the lowest aspect ratio, 0.305 ± 0.008 . The alcohol binding groups on $T6_{1,2,3}$ are in close proximity to one another, located on the first, second (α -C), and third carbons (β -C); however, when we examined its isomer $T6_{1,2,6}$, where the alcohol on the β -C is shifted to the sixth carbon, there was a reduction in ZGM efficacy (i.e., a higher aspect ratio, 0.43 ± 0.04). This suggests the spatial separation between alcohol moieties along the ZGM backbone influences its binding to the LTL (001) surface. We also compared $D5_{1,2}$ with its isomer $D5_{1,5}$ in which the alcohol is repositioned from the α -C to the fifth carbon. Interestingly, this adjustment in spatial sequence did not affect ZGM efficacy. In fact, the following four ZGMs produced LTL crystals with nearly identical aspect ratios: $T6_{1,2,6}$, $D6_{1,2}$, $D5_{1,2}$, and $D5_{1,5}$ (see Table 1 for ZGM molecular structures). Collectively, these studies suggest that polyols are more effective modifiers when the alcohols are located on the first and third carbons. Placement of an alcohol on the α -C is apparently less effective, potentially due to steric constraints. For instance, it is feasible that 1,2-polyols cannot adopt structural conformations that enable adjacent alcohols to cooperatively bind to hydroxyl groups on the (001) surface. Likewise, it is reasonable to suggest that the spatial separation of alcohol groups in 1,3-polyols facilitates their binding to LTL crystals, which is analogous to findings by Sievers and co-workers who reported enhanced adsorption of 1,3-diols on γ - Al_2O_3 surfaces.⁶⁶ Our hypothesis seemingly holds true for LTL ZGMs even when placement of an alcohol on a β -C reduces alkyl lengths below the aforementioned $(CH_2)_3$ threshold. For example, we observed that $D4_{1,3}$ is a slightly more effective modifier than $D4_{1,2}$. Although the former has a shorter alkyl sequence, it possesses a β -carbon alcohol, which ostensibly has a greater influence on the LTL [001] growth rate. Collectively, this systematic study of polyols illustrates that a subtle difference in ZGM molecular structure markedly influences its efficacy.

Our studies also revealed that ZGMs with primary alcohol and amine binding moieties induce similar effects (within experimental error) on LTL aspect ratio, as illustrated by the comparison of structurally equivalent P3/A3 and P4/A4 pairs in Figure 4. The lack of commercially available di- and triamines prevented a more rigorous comparison of primary amines and alcohols; however, examination of readily available ZGMs with secondary amines (e.g., triethylenetetramine) and ethers (e.g., diethyl ether) revealed that these chemical moieties were less effective than primary amines and alcohols, respectively (see Table S4). This observation is in stark contrast to our previous work⁴⁵ where we reported that ZGMs with secondary amines, such as spermine, were effective modifiers of MFI zeolite. Interestingly, we found that some of the most effective ZGMs for MFI crystallization,⁴⁵ including tributylphosphine oxide, produce only marginal effects on LTL crystal aspect ratio (see Table S5). Our comparative study of LTL and MFI crystallization in the presence of select modifiers shows that

Table 2. Comparison of Monomer and Polymer ZGM Efficacy

Zeolite Growth Modifiers	Structure	wt % ^a	MW (g·mol ⁻¹)	Aspect Ratio
Control	1.7 ± 0.1
1-ethyl-1-methylpyrrolidinium-bromide, (EMPB)		2.81	194	2.5 ± 0.1
poly(diallyldimethylammonium chloride), (PDDAC)		2.34	150,000	9.1 ± 0.4

^aMoles of quaternary amine groups were fixed.

an effective ZGM for one zeolite may not display similar specificity and/or efficacy for other framework types, which further emphasizes the subtle nuances of ZGM–zeolite molecular recognition.

Here we also examined the role of electrostatic interactions using ZGMs with positively charged quaternary amines (Table 2). It is well established that organic structure-directing agents in zeolite synthesis commonly possess these functional groups;⁶⁷ therefore, we avoided using quaternary amines, such as tetraalkylammonium ions, that could promote the formation of unwanted crystal polymorphs. Instead, we selected two quaternary amines not commonly used as SDAs: the polymer poly(diallyldimethylammonium chloride) (PDDAC) and 1-ethyl-1-methylpyrrolidinium bromide (EMPB). The monomer of PDDAC is not commercially available; thus, we used an analogue with structural similarity, EMPB, as a quasi-monomer. Of particular interest is the fact that these quaternary amines preferentially bind to LTL {100} surfaces. As shown in Figure 1f, ZGM binding to {100} surfaces inhibits growth normal to the plane, thereby shifting the dominant growth rate along the axial [001] direction. This results in the formation of rod-like LTL crystals with high aspect ratio (Figure 1c, $L/D > \sim 10$). It is reasonable to suggest that electrostatic interactions contribute to the adsorption of positively charged quaternary amines, such as PDDAC and EMPB, to negatively charged LTL crystal surfaces. It is known that zeolite surfaces possess anionic charges derived from either dissociated silanol groups (SiOH) or tetrahedral (T) sites occupied by Al in the crystal framework. The number of Al T-sites is relatively high in LTL crystals, which typically have a silicon-to-aluminum ratio (SAR) between 2.5 and 3.6^{60,68} (e.g., elemental analysis of control crystals revealed a SAR value of 3.3). The density of T atoms on LTL (001) and {100} surfaces is approximately 8.4 and 10.5 sites/nm², respectively (see Figure 2). If the negative charge on crystal surfaces was derived solely from the number of Al sites, the {100} surfaces, which exhibit higher T-atom density, would be the most negatively charged; however, we must also account for dissociated silanol groups. As shown in Figure 2d, 50% of T atoms on the (001) surface have hydroxyl groups (either SiOH or AlOH) compared to only 14% on {100} surfaces. Without knowledge of the spatial positioning of Si atoms in the crystal framework, an exact surface charge density is difficult to approximate. While it is feasible that {100} surfaces have higher charge density, additional factors may also contribute to the preferential binding of PDDAC and EMPB to these surfaces. For instance, the disparate topologies of LTL (001) and {100} surfaces govern the total number of bonds formed between

ZGM moieties and hydroxyl groups on each zeolite interface; thus, it is possible that PDDAC and EMPB can orient on the {100} plane to maximize the electrostatic interactions between anionic groups on the crystal surface and cationic groups within the ZGM. The close proximity of hydroxyl groups on the (001) surface may impose steric constraints that hinder adsorption of bulky modifiers, such as PDDAC, compared to {100} surfaces where the hydroxyl groups, albeit fewer, are more dispersed. This could explain an observation that we did not previously mention in the analysis of polyols, which is that glycerol (T_{3,1,2,3}) preferentially binds to {100} surfaces and increases the LTL aspect ratio by 25% (see Figure 4). This anomaly among alcohols in Table 1 cannot be rationalized by disparate hydroxyl densities on the two LTL crystal planes, but rather differences in the spatial arrangement of hydroxyl groups on these surfaces.

Our investigation of quaternary amines also revealed that PDDAC yields a 4-fold increase in LTL crystal aspect ratio relative to EMPB (see Table 2). This is consistent with phenomena observed in biomineralization (e.g., calcification) where polymeric modifiers are reportedly more effective growth inhibitors than their respective monomeric counterparts. Examples include *in vitro* crystallization of calcium oxalate where Ward and co-workers⁶⁹ hypothesized that the cooperative action of proximal binding groups on macromolecules, such as polypeptides, enhanced their adsorption to crystal surfaces and improved their potency relative to smaller molecules (e.g., amino acids). Indeed, our studies show that PDDAC exhibits much higher potency compared to EMPB and other ZGMs tested in Table 1. The potency of ZGMs was assessed by systematically varying their concentration in LTL growth solutions. Our studies indicate that dramatic changes in LTL crystal habit can be achieved using a very low quantity of modifier. In Figure 5, we compare the potency of three ZGMs: P2, EMPB, and PDDAC. Increased ZGM concentrations resulted in a monotonic change in crystal aspect ratio, which reached a plateau at some threshold ZGM weight percent, above which additional increases in concentration resulted in negligible changes in aspect ratio. This trend was observed for all three ZGMs tested, with threshold values of 6 wt% for

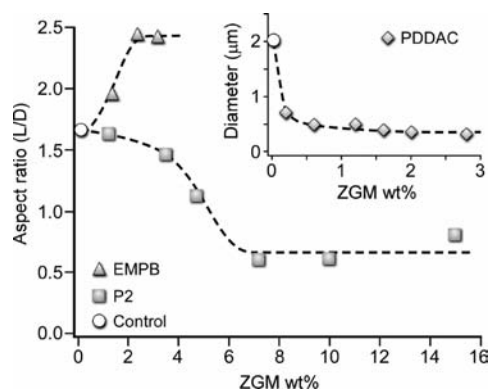


Figure 5. Concentration dependence of ZGM efficacy. Bulk crystallization in the presence of P2 and EMPB at varying weight percents reveals a decrease and increase in LTL crystal aspect ratio, respectively. (Inset) Effect of PDDAC weight percent on LTL crystal size. For PDDAC we report changes in crystal diameter rather than aspect ratio since many LTL crystals at higher L/D ratios appeared broken in electron micrographs (see Figure S5). Each symbol is the average of 30 measurements using SEM images from a single crystal batch, and dashed lines are interpolations of experimental data.

ethanol (P2), 2 wt% for EMPB, and 0.2 wt% for PDDAC (i.e., an order of magnitude lower than other ZGMs).

The general trends in Figure 5 are consistent with a Langmuirian model where modifier adsorption to crystal surfaces leads to higher localized concentrations (compared to bulk solution) that can readily perturb solute attachment to active growth sites on LTL surfaces. This kinetic description contrasts thermodynamic arguments in the literature that refer to organic additives in LTL synthesis as cosolvents^{32,33} that alter the surface free energy of crystals. To our knowledge, there are no theoretical models that predict solvent effects on zeolite crystal habit. Doherty⁷⁰ and Davey⁷¹ have proposed models for organic crystallization (e.g., adipic and succinic acids) that account for the presence of solvent in the vicinity of growth sites (i.e., kink sites) using a mean approximation of crystal and solvent contributions. If we were to apply the fundamental premise of these models to zeolites, each kink site on the surface of LTL crystals would be in contact with few alcohols. For example, a 6 wt% ethanol solution (i.e., threshold concentration of P2 in Figure 5) has a very high water-to-ethanol molar ratio (ca. 40 H₂O:1.0 P2). We argue it is unlikely that such a minute amount of ethanol near the zeolite surface would have such a large impact on its surface free energy, and therefore cannot account for the observed changes in crystal morphology. As such, we propose that prior references to zeolite additives as cosolvents are, in fact, reporting a kinetic effect of ZGMs. Likewise, we postulate that other studies of zeolite shape modification classifying organics in zeolite synthesis as space fillers⁴⁴ or Al-binding ligands^{30,35} may be observing a similar phenomenon.

In this study, we explored a synergistic approach that couples ZGMs with the judicious adjustment of synthesis parameters as a route to tailor crystal habit beyond what is attainable in the absence of ZGMs. Other groups have reported that the adjustment of synthesis conditions influences LTL crystal size and habit. Critical factors identified in the literature include the use of SDAs and various sources of SiO₂ and Al₂O₃, as well as changes in solution SAR, pH, water content, and synthesis temperature and time.^{25–28} In general, the LTL crystal aspect ratio decreases with (i) decreased Al content,²⁶ (ii) decreased water content,^{26,28} and (iii) reduced temperature.²⁸ Concentrated sols and lower temperatures produce nanosized LTL crystals (ca. 40 nm),^{8,24} while modifications in solution composition yield high aspect ratio LTL rods (average $L/D = 10$).^{26–28} Here we chose to investigate the effect of ZGMs in combination with changes in water content and temperature.

The effect of water content was explored by adjusting the $x\text{H}_2\text{O}:1.0\text{ Al}_2\text{O}_3$ molar ratio of synthesis solutions in the range $830 \leq x \leq 1230$. In the absence of ZGMs, the LTL crystal aspect ratio varied between 1 and 3 (see Figure S6), whereas the use of ZGMs extended this range by a factor of 3 (i.e., aspect ratio = 0.3–10). Modifications in LTL crystal habit were primarily attributed to the action of the ZGM, yet the coupled effect of ZGM and water content did produce an additional 10–20% change in aspect ratio. A more pronounced synergistic effect was achieved by reducing the synthesis temperature from 180 °C (nominal condition) to 100 °C in the presence of T6_{1,2,6}. The coupled effect of lower temperature and ZGM led to a 4-fold reduction in crystal aspect ratio (see Figure 6a). To our knowledge, this is the lowest reported length-to-diameter aspect ratio of LTL crystals (see Table 3 for a comparison of our results with those in the literature).

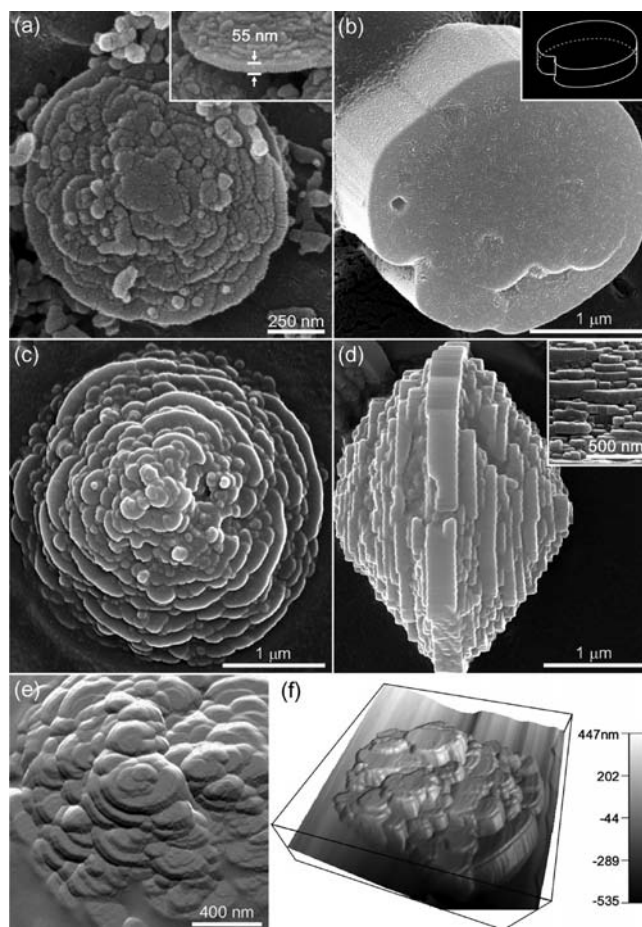


Figure 6. Scanning electron micrographs of LTL crystals grown in the presence of 17 wt% T6_{1,2,6} at (a) 100 °C and (b) 180 °C exhibit different surface features (rough and smooth, respectively). Higher temperature produced centroid shapes (b, inset). Synthesis in the presence of P4 produced crystals with biconical shape (c,d). High-magnification images (d, inset) highlight the variation in step height (see Figure S12 for a low-magnification image showing the reproducibility of crystal habit). AFM images of LTL crystals in (e) deflection and (f) height mode reveal a polydisperse distribution of step bunches with variable height on the (001) surface. Images c–f were taken of crystals grown in the presence of 10 wt% P4.

As previously mentioned, the synthesis of low aspect ratio LTL crystals is a design objective for engineering high performance materials with (i) reduced [001] dimension to minimize the internal diffusion path length, (ii) tailored morphology to enhance trapping efficiency (e.g., guest–host systems), and (iii) increased (001) surface area to improve sorbate access to pores. As shown in Table 3, it is possible to synthesize LTL crystals in the absence of ZGMs with a diffusion path length of 40 nm or less;^{8,24} however, these crystals tend to have extremely small (001) surface area (ca. $10^{-4}\ \mu\text{m}^2/\text{particle}$). Past studies report disc (or so-called clam-shaped) LTL crystals with roughened surfaces, approximate [001] thicknesses of 200–650 nm, and average (001) surface areas of 10^{-1} – $10^0\ \mu\text{m}^2/\text{particle}$.^{8,24,27,29,30,33} In the presence of ZGMs, we were able to synthesize LTL platelets with diffusion path lengths approximately 2-fold less than previously reported, while simultaneously preserving high (001) surface area (ca. $10^0\ \mu\text{m}^2/\text{particle}$). It is reasonable to expect that even further reduction in platelet thickness (without sacrificing external porous surface area) can be achieved via a more rigorous

Table 3. Comparison of LTL Crystal Properties between Our Work and Select Literature References

ref ^a	synthesis composition (Al ₂ O ₃ :SiO ₂ :K ₂ O:H ₂ O)	T (°C)	time (h)	ZGM	AR _(L/D) ^b	L _[001] ^c (μm)	SA ₍₀₀₁₎ ^d (μm ² /part.)
our work	1:20:10.2:1030 (control)	180	72		1.7	4.0	10 ¹
	1:20:10.2:1030	180	72	T6 _{1,2,6}	0.4	1.3	10 ¹
	1:20:10.2:1030	100	168		0.4	0.38	10 ⁰
	1:20:10.2:1030	100	168	T6 _{1,2,6}	0.1	0.11	10 ⁰
8	1:10:3.5:160 (clam)	150	120		0.7	0.65	10 ⁰
27	1:30:10.9 ^e :416	160	48		0.3	0.35	10 ⁰
29	1:15:10.0:250	160	144		0.5	0.30	10 ⁻¹
30	1:9.7:3.3:161	120	144	H3 _{tea} ^f	0.2	0.30	10 ⁰
33	1:20:10.2:950	150	72	P2	0.3	0.20	10 ⁻¹
24	1:20:10.0:400 (nano)	175	4		2.7	0.04	10 ⁻⁴

^aLiterature references. ^bAR = length-to-diameter aspect ratio, L/D. ^cL = length of LTL crystals in the [001] direction. ^dSA = surface area of basal (001) faces per particle (order of magnitude). ^eWe were unable to synthesize similar LTL crystals using our synthesis composition and triethanol amine (H3_{tea}) as a ZGM. ^fTotal alkaline content is 5.4 K₂O + 5.5 Na₂O = 10.9 M₂O.

exploration of optimal ZGM and synthesis parameter combinations.

Atomic force microscopy (AFM) has proven to be a useful tool capable of elucidating crystal growth mechanisms, characterizing adsorbate-crystal interactions, and quantifying anisotropic rates of layer growth in both the absence and presence of modifiers.^{44,45,72–77} Anderson and co-workers used AFM to probe the surface topography of various zeolite framework types, including several studies focused on the investigation of LTL growth mechanisms. In the present work, we use AFM in combination with scanning electron microscopy (SEM) to examine the effect(s) of ZGMs on the topography of LTL (001) surfaces. Control crystals prepared in the absence of ZGMs exhibit smooth (001) surfaces (see Figure 1a), whereas those prepared with ZGMs yield a myriad of features. In the presence of T6_{1,2,6} at 100 °C, basal surfaces exhibit a relatively high density of islands (Figure 6a); however, the same growth solution at 180 °C produce smoother surfaces with fewer islands (Figure 6b). Moreover, syntheses with 1,2-pentanediol (DS_{1,2}) result in LTL crystals with smooth (001) surfaces, while those with butylamine (A4) produce a significantly higher number of islands (additional examples are provided in Figure S11). Collectively, we observed that different ZGMs and/or adjustments to synthesis parameters tune island density on the (001) surface. Furthermore, ZGMs were capable of producing different LTL platelet geometries, such as rounded edges (Figure 6a), faceted hexagonal edges (see Figure S3), and centroid-like shapes (Figure 6b).

Another distinct outcome of this study was the formation of biconical LTL crystals using *n*-butanol (P4). A top view of these crystals (Figure 6c) shows a radial distribution of islands emanating from the center of the basal plane. A side profile of these crystals (Figure 6d) reveals layers of varying height (also evident in low-magnification SEM images, Figure S12). The AFM deflection image in Figure 6e depicts a typical island density, while the 3D height image in Figure 6f highlights the vast distribution of layer heights. AFM images of (001) surfaces reveal the presence of islands greater than 10 nm in height and virtually no single steps (i.e., 0.76 nm height equivalent to the *c*-axis unit cell dimension). This suggests that polydisperse distributions of islands are likely caused by 3D nucleation as layers grow on the crystal surface. ZGM promotion of island density on LTL (001) surfaces is in stark contrast to our previous findings for MFI-type zeolite, which showed that ZGM binding to MFI basal surfaces inhibited layer nucleation on advancing steps. Distinct variations in LTL crystal

topography for syntheses with different ZGMs likely reflect the inherent binding mode of each modifier to the (001) surface. Elucidating the specific factors governing ZGM–zeolite binding modes is challenging without the aid of atomistic or molecular models. Nevertheless, this study exemplifies the unparalleled ability of ZGMs to alter LTL surface architecture, which has broader implications for designing advanced zeolitic materials. For example, Resasco and co-workers⁸ examined *n*-octane aromatization using Pt-LTL catalysts with surfaces similar to those in Figure 6a,b. They reported that LTL crystals with smoother basal surfaces improved catalyst activity, selectivity, and lifetime. To this end, our synthesis scheme using ZGMs to tailor surface roughness with concomitant optimization of crystal habit and external porous surface area is advantageous for the rational design of improved catalysts, and has the potential to enhance the design of LTL zeolites for additional applications (e.g., biomedical and photonic devices). To our knowledge, such versatility in zeolite crystal engineering has not been previously demonstrated.

CONCLUSION

In conclusion, we have shown that a facile strategy can be employed to tailor the morphology and surface architecture of zeolite LTL crystals. Our studies reveal general physicochemical factors governing ZGM efficacy and binding affinity. Notably, quaternary amines bind preferentially to {100} surfaces, while 1,3-polyols with alkyl segments of (CH₂)₃ or longer most effectively adsorb on (001) surfaces. The judicious selection of modifiers with specificity for either the (001) or {100} surfaces moderates the length-to-diameter aspect ratio of LTL crystals over 3 orders of magnitude. This flexibility in material design holds considerable promise for a broad range of industrial-scale applications. As mentioned, the synthesis of thin platelets with minimal diffusion path length and large external porous surface area can optimize properties critical in catalysis, photonic devices, and biomedical applications. Moreover, high aspect ratio rod-like crystals may prove useful in the future as microcapillary devices for light harvesting antenna and luminescent labeling. As such, we believe this commercially viable strategy is a paradigm in zeolite synthesis capable of producing unrivaled materials that have eluded more conventional techniques.

■ ASSOCIATED CONTENT

■ Supporting Information

Details of XRD, TGA, AFM, SEM, and bulk crystallization measurements; L/D aspect ratio calculations; $\{100\}$ surface identification; complete list of all ZGMs tested; hydrophobicity calculations; effect of water content and temperature variation; efficacy of ZGMs with secondary amines and ethers; and comparison of modifiers for LTL and MFI. This material is available free of charge via the Internet at <http://pubs.acs.org>.

■ AUTHOR INFORMATION

Corresponding Author

jrimer@central.uh.edu

Notes

The authors declare no competing financial interest.

■ ACKNOWLEDGMENTS

We acknowledge financial support from the National Science Foundation (CBET-1151098), the American Chemical Society Petroleum Research Fund (52422-DNIS), and the Welch Foundation (E-1794). We thank the Department of Nanomedicine SEM Core in the Methodist Hospital Research Institute for instrument access.

■ REFERENCES

- (1) Corma, A. *J. Catal.* **2003**, *216*, 298.
- (2) Sun, J.; Bonneau, C.; Cantin, A.; Corma, A.; Diaz-Cabanas, M. J.; Moliner, M.; Zhang, D.; Li, M.; Zou, X. *Nature* **2009**, *458*, 1154.
- (3) Drews, T. O.; Tsapatsis, M. *Curr. Opin. Colloid Interface Sci.* **2005**, *10*, 233.
- (4) Martínez, C.; Corma, A. *Coord. Chem. Rev.* **2011**, *255*, 1558.
- (5) Cundy, C. S.; Cox, P. A. *Chem. Rev.* **2003**, *103*, 663.
- (6) Maldonado, M.; Oleksiak, M. D.; Chinta, S.; Rimer, J. D. *J. Am. Chem. Soc.* **2012**, *135*, 2641.
- (7) Davis, R. J. *Heterogen. Chem. Rev.* **1994**, *1*, 41.
- (8) Trakamroek, S.; Jongpatiwut, S.; Rirksomboon, T.; Osuwan, S.; Resasco, D. E. *Appl. Catal. a-Gen.* **2006**, *313*, 189.
- (9) Jentoft, R. E.; Tsapatsis, M.; Davis, M. E.; Gates, B. C. *J. Catal.* **1998**, *179*, 565.
- (10) Joshi, P. N.; Bandyopadhyay, R.; Awate, S. V.; Shiralkar, V. P.; Rao, B. S. *React. Kinet. Catal. Lett.* **1994**, *53*, 231.
- (11) Miller, J. T.; Agrawal, N. G. B.; Lane, G. S.; Modica, F. S. *J. Catal.* **1996**, *163*, 106.
- (12) Cortright, R. D.; Dumesic, J. A. *Appl. Catal. a-Gen.* **1995**, *129*, 101.
- (13) Barrer, R. M.; Galabova, I. M. *Adv. Chem. Ser.* **1973**, 356.
- (14) Lee, T. P.; Saad, B.; Ng, E. P.; Salleh, B. *J. Chromatogr. A* **2012**, *1237*, 46.
- (15) Koeppe, R.; Bossart, O.; Calzaferri, G.; Sariciftci, N. S. *Sol. Energy Mater. Sol. C* **2007**, *91*, 986.
- (16) Calzaferri, G.; Meallet-Renault, R.; Bruhwiler, D.; Pansu, R.; Dolamic, I.; Dienel, T.; Adler, P.; Li, H. R.; Kunzmann, A. *Chemphyschem* **2011**, *12*, 580.
- (17) Calzaferri, G.; Huber, S.; Maas, H.; Minkowski, C. *Angew. Chem., Int. Ed.* **2003**, *42*, 3732.
- (18) Ruiz-Sanchez, A. J.; Montanez, M. I.; Mayorga, C.; Torres, M. J.; Kehr, N. S.; Vida, Y.; Collado, D.; Najera, F.; De Cola, L.; Perez-Inestrosa, E. *Curr. Med. Chem.* **2012**, *19*, 4942.
- (19) Tsotsalas, M. M.; Kopka, K.; Luppi, G.; Wagner, S.; Law, M. P.; Schafers, M.; De Cola, L. *ACS Nano* **2010**, *4*, 342.
- (20) Li, Z.; Hüve, J.; Krampe, C.; Luppi, G.; Tsotsalas, M.; Klingauf, J.; De Cola, L.; Riehemann, K. *Small* **2013**, DOI: 10.1002/sml.201201702.
- (21) Li, Z.; Luppi, G.; Geiger, A.; Josel, H. P.; De Cola, L. *Small* **2011**, *7*, 3193.

- (22) Kehr, N. S.; Riehemann, K.; El-Gindi, J.; Schafer, A.; Fuchs, H.; Galla, H. J.; De Cola, L. *Adv. Funct. Mater.* **2010**, *20*, 2248.
- (23) Veiga-Gutierrez, M.; Woerdemann, M.; Prasetyanto, E.; Denz, C.; De Cola, L. *Adv. Mater.* **2012**, *24*, 5199.
- (24) Tsapatsis, M.; Lovallo, M.; Okubo, T.; Davis, M. E.; Sadakata, M. *Chem. Mater.* **1995**, *7*, 1734.
- (25) Ko, Y. S.; Ahn, W. S. *Powder Technol.* **2004**, *145*, 10.
- (26) Lee, Y. J.; Lee, J. S.; Yoon, K. B. *Micropor. Mesopor. Mater.* **2005**, *80*, 237.
- (27) Ruiz, A. Z.; Bruhwiler, D.; Ban, T.; Calzaferri, G. *Monatsh. Chem.* **2005**, *136*, 77.
- (28) Larlus, O.; Valtchev, V. P. *Chem. Mater.* **2004**, *16*, 3381.
- (29) Megelski, S.; Calzaferri, G. *Adv. Funct. Mater.* **2001**, *11*, 277.
- (30) Ban, T.; Saito, H.; Naito, M.; Ohya, Y.; Takahashi, Y. *J. Porous Mater.* **2007**, *14*, 119.
- (31) Lee, S.; Shantz, D. F. *Chem. Commun.* **2004**, 680.
- (32) Gaona-Gomez, A.; Cheng, C. H. *Micropor. Mesopor. Mater.* **2012**, *153*, 227.
- (33) Gomez, A. G.; de Silveira, G.; Doan, H.; Cheng, C. H. *Chem. Commun.* **2011**, *47*, 5876.
- (34) Carr, C. S.; Shantz, D. F. *Chem. Mater.* **2005**, *17*, 6192.
- (35) Sano, T.; Wakabayashi, S.; Oumi, Y.; Uozumi, T. *Micropor. Mesopor. Mater.* **2001**, *46*, 67.
- (36) Gao, F. F.; Li, X. T.; Zhu, G. S.; Qui, S. L.; Wei, B.; Shao, C. L.; Terasaki, O. *Mater. Lett.* **2001**, *48*, 1.
- (37) Scott, G.; Thompson, R. W.; Dixon, A. G.; Sacco, A. *Zeolites* **1990**, *10*, 44.
- (38) Shao, C. L.; Li, X. T.; Qiu, S. L.; Xiao, F. S.; Terasaki, O. *Micropor. Mesopor. Mater.* **2000**, *39*, 117.
- (39) Iwasaki, A.; Sano, T.; Kiyozumi, Y. *Micropor. Mesopor. Mater.* **1998**, *25*, 119.
- (40) Kinrade, S. D.; Del Nin, J. W.; Schach, A. S.; Sloan, T. A.; Wilson, K. L.; Knight, C. T. *Science* **1999**, *285*, 1542.
- (41) Davis, M. E.; Lobo, R. F. *Chem. Mater.* **1992**, *4*, 756.
- (42) Na, K.; Jo, C.; Kim, J.; Cho, K.; Jung, J.; Seo, Y.; Messinger, R. J.; Chmelka, B. F.; Ryoo, R. *Science* **2011**, *333*, 328.
- (43) Lai, Z.; Bonilla, G.; Diaz, I.; Nery, J. G.; Sujaoti, K.; Amat, M. A.; Kokkoli, E.; Terasaki, O.; Thompson, R. W.; Tsapatsis, M.; Vlachos, D. G. *Science* **2003**, *300*, 456.
- (44) Brent, R.; Lobo, A. J. W.; Lewis, D. W.; Anderson, M. W. *J. Phys. Chem. C* **2010**, *114*, 18240.
- (45) Lupulescu, A. I.; Rimer, J. D. *Angew. Chem., Int. Ed.* **2012**, *51*, 3345.
- (46) Weissbuch, I.; Addadi, L.; Lahav, M.; Leiserowitz, L. *Science* **1991**, *253*, 637.
- (47) Addadi, L.; Vanmil, J.; Weissbuch, I.; Berkovitchyellin, Z.; Leiserowitz, L.; Lahav, M. *Chem. Scr.* **1985**, *25*, 91.
- (48) De Yoreo, J. J.; Dove, P. M. *Science* **2004**, *306*, 1301.
- (49) Elhadji, S.; Salter, E. A.; Wierzbicki, A.; De Yoreo, J. J.; Han, N.; Dove, P. M. *Cryst. Growth Des.* **2006**, *6*, 197.
- (50) Chen, C.-L.; Qi, J.; Zuckermann, R. N.; DeYoreo, J. J. *J. Am. Chem. Soc.* **2011**, *133*, 5214.
- (51) Wang, L.; Nancollas, G. H. *Chem. Rev.* **2008**, *108*, 4628.
- (52) Meldrum, F. C.; Cölfen, H. *Chem. Rev.* **2008**, *108*, 4332.
- (53) Doxey, A. C.; Yaish, M. W.; Griffith, M.; McConkey, B. J. *Nat. Biotechnol.* **2006**, *24*, 852.
- (54) Graether, S. P.; Kuiper, M. J.; Gagne, S. M.; Walker, V. K.; Jia, Z.; Sykes, B. D.; Davies, P. L. *Nature* **2000**, *406*, 325.
- (55) Farmanesh, S.; Chung, J.; Chandra, D.; Sosa, R. D.; Karande, P.; Rimer, J. D. *J. Cryst. Growth* **2013**, in press.
- (56) Rimer, J. D.; An, Z.; Zhu, Z.; Lee, M. H.; Goldfarb, D. S.; Wesson, J. A.; Ward, M. D. *Science* **2010**, *330*, 337.
- (57) Mavredaki, E.; Neville, A.; Sorbie, K. S. *Cryst. Growth Des.* **2011**, *11*, 4751.
- (58) Dickerson, M. B.; Sandhage, K. H.; Naik, R. R. *Chem. Rev.* **2008**, *108*, 4935.
- (59) Ohsuna, T.; Horikawa, Y.; Hiraga, K.; Terasaki, O. *Chem. Mater.* **1998**, *10*, 688.

- (60) Ohsuna, T.; Slater, B.; Gao, F. F.; Yu, J. H.; Sakamoto, Y.; Zhu, G. S.; Terasaki, O.; Vaughan, D. E. W.; Qiu, S. L.; Catlow, C. R. A. *Chem.—Eur. J.* **2004**, *10*, 5031.
- (61) International Zeolite Association, 2007; <http://www.iza-online.org/>.
- (62) Xiong, R. C.; Sandler, S. I.; Vlachos, D. G. *J. Phys. Chem. C* **2011**, *115*, 18659.
- (63) Xiong, R. C.; Sandler, S. I.; Vlachos, D. G. *Langmuir* **2012**, *28*, 4491.
- (64) Mallon, E. E.; Bhan, A.; Tsapatsis, M. *J. Phys. Chem. B* **2010**, *114*, 1939.
- (65) Mallon, E. E.; Babineau, I. J.; Kranz, J. I.; Guefrachi, Y.; Siepmann, J. I.; Bhan, A.; Tsapatsis, M. *J. Phys. Chem. B* **2011**, *115*, 11431.
- (66) Copeland, J. R.; Shi, X.-R.; Sholl, D. S.; Sievers, C. *Langmuir* **2012**, *29*, 581.
- (67) Lobo, R. F.; Zones, S. I.; Davis, M. E. *J. Incl. Phenom. Mol. Recognit. Chem.* **1995**, *21*, 47.
- (68) Breck, D. W. *Zeolite Molecular Sieves: Structure, Chemistry and Use*; Wiley: New York, 1974.
- (69) Guo, S.; Ward, M. D.; Wesson, J. A. *Langmuir* **2002**, *18*, 4284.
- (70) Winn, D.; Doherty, M. F. *AIChE J.* **1998**, *44*, 2501.
- (71) Davey, R. J.; Mullin, J. W.; Whiting, M. J. L. *J. Cryst. Growth* **1982**, *58*, 304.
- (72) Brent, R.; Anderson, M. W. *Stud. Surf. Sci. Catal.* **2008**, *174*, 909.
- (73) Brent, R.; Anderson, M. W. *Angew. Chem., Int. Ed.* **2008**, *47*, 5327.
- (74) Brent, R.; Cubillas, P.; Stevens, S. M.; Jelfs, K. E.; Umemura, A.; Gebbie, J. T.; Slater, B.; Terasaki, O.; Holden, M. A.; Anderson, M. W. *J. Am. Chem. Soc.* **2010**, *132*, 13858.
- (75) Friddle, R. W.; Battle, K.; Trubetskoy, V.; Tao, J.; Salter, E. A.; Moradian-Oldak, J.; De Yoreo, J. J.; Wierzbicki, A. *Angew. Chem., Int. Ed.* **2011**, *50*, 7541.
- (76) Friddle, R. W.; Noy, A.; De Yoreo, J. J. *Proc. Natl. Acad. Sci. U.S.A.* **2012**, *109*, 13573.
- (77) Friddle, R. W.; Weaver, M. L.; Qiu, S. R.; Wierzbicki, A.; Casey, W. H.; De Yoreo, J. J. *Proc. Natl. Acad. Sci. U.S.A.* **2010**, *107*, 11.